Review

International Journal of Modern Physics B
Vol. 26, No. 13 (2012) 1230006 (21 pages)

DOI: 10.1142/S021797921230006X

World Scientific
www.worldscientific.com

PRINCIPLES OF SINGLE-MOLECULE MANIPULATION AND ITS APPLICATION IN BIOLOGICAL PHYSICS

WEI-HUNG CHEN*,†, JONATHAN D. WILSON*, SITHARA S. WIJERATNE*, SARAH A. SOUTHMAYD*, KUAN-JIUH LIN† and CHING-HWA KIANG*,‡

*Department of Physics and Astronomy, Rice University, Houston, Texas 77005, USA
†Department of Chemistry, National Chung Hsing University, Taichung, Taiwan
‡chkiang@rice.edu

Received 8 March 2012
Published 30 April 2012

Recent advances in nanoscale manipulation and piconewton force detection provide a unique tool for studying the mechanical and thermodynamic properties of biological molecules and complexes at the single-molecule level. Detailed equilibrium and dynamics information on proteins and DNA have been revealed by single-molecule manipulation and force detection techniques. The atomic force microscope (AFM) and optical tweezers have been widely used to quantify the intra- and inter-molecular interactions of many complex biomolecular systems. In this article, we describe the background, analysis, and applications of these novel techniques. Experimental procedures that can serve as a guide for setting up a single-molecule manipulation system using the AFM are also presented.

Keywords: Single-molecule; AFM; biomolecule.

1. Introduction

Over the last few years, studying the role of mechanics in biomolecules has helped us gain insight into the mechanochemical transduction inside and outside cells.[1,2] The mechanical properties of biomolecules may also play an essential role in understanding the interplay between mechanics and biochemistry. Since Isaac Newton wrote his three laws of motion more than three centuries ago, great progress has been made in mechanics. There is now increasing evidence that mechanics plays an important role in advancing life science and medicine.[3] The connection between mechanics and biological functions has become a subject of broad interest.

Like an error-free factory at the nanoscale, molecular machines in biological systems perform specific functions induced by tiny forces. When forces are applied to these biomolecules, their conformations change in response to the load. It is well-established that the three-dimensional structure of the biomolecule defines

‡Corresponding author.

its function. However, the conformations of biomolecules change constantly within their biological systems, thus studying biomolecular properties *via* mechanics will illuminate their dynamics and functions. Information about the kinetics of the conformational changes will allow us to understand how their structural changes trigger biological reactions. Recently, due to advances in nanotechnology, methods such as AFM and optical tweezers for measuring the forces in individual molecules have been developed to investigate the kinetics of these conformational changes, thereby linking their mechanical response with biochemical function.

1.1. *Mechanics of biological systems*

1.1.1. *Cell mechanotransduction*

Cells, the basic units of life, are complex biological systems. Recently, studies have shown that the mechanical environment may play a regulatory role in cellular functions.[4–7] Therefore, studying the mechanical properties of cells may shed light on their biological functions. One example is bone tissue, which is continuously constructed and destroyed by two bone cells, osteoblast and osteoclast.[8,9] The dynamic equilibrium of this bone remodeling cycle controls bone gain and loss, and dysregulation of this equilibrium is linked to osteoporosis.[9] Recent studies on astronauts have suggested that mechanical force plays an important role in the regulation of bone metabolism.[10] These studies reveal that working in weightless environments can cause a loss of bone density at up to 1–2% each month,[6] ten times faster than that of osteoporosis patients on Earth. Weight-bearing exercises effectively slow this decay rate, implying that force (gravity) is a key regulator of bone metabolism.[11]

Another well-known example of mechanical regulation is the endothelial cell, which forms the interior surface of blood vessels and responds rapidly to mechanical forces. Studies have shown that vascular morphology and physiology are largely determined by blood flow,[5,12] and that endothelial cells are the components that mediate this effect. In a healthy blood vessel, laminar shear forces from blood flow make endothelial cells align along the walls of the vessel. In contrast, slow or turbulent blood flow activates endothelial cells and increases their turnover rate, resulting in substantial disordered cells, cell retraction, or cell loss and hence the early development of vascular diseases, such as atherosclerosis.

1.1.2. *Elasticity of biomolecules*

To determine how cells convert mechanical forces into biochemical signals, an investigation of the biomolecules inside the cells is necessary. A cell is wrapped with the plasma membrane and braced by the cytoskeleton, which consists of filament proteins that serve as intracellular scaffolds to support the cell's shape[4] (see Fig. 1). The conformational changes of the cytoskeleton alter the tension and the structure of the cell. In a physiological environment, cells are attached to the extracellular

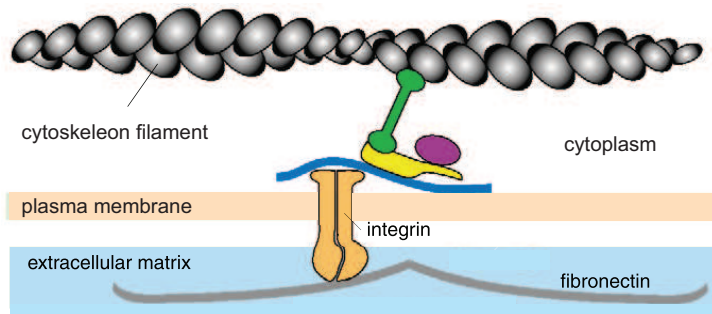

Fig. 1. A cell attaches to the ECM through the binding between ECM proteins, such as fibronectin and integrin and the intracellular domain, which couples to the cytoskeleton.[4] Adapted from Ref. 4.

matrix (ECM) through the binding between the ECM proteins and the receptor proteins on the cell surface.[13]

Integrin, a transmembrane protein attached to the cell cytoskeleton, is crucial to the adhesive stability between the cell and the ECM or other cells. Since integrins provide the mechanical linkage between the cell cytoskeleton and ECM, cytoskeleton systems can sense mechanical forces through integrin-mediated cell-ECM interactions and change their structure to generate intracellular force to resist the load.[14] How the mechanical properties of cytoskeleton proteins affect the biochemical reactions inside the cell remains unknown. However, it has been suggested that the deformation of the cytoskeleton might modify its affinity with the proteins attached to it.[15] This affinity modification could then induce the alteration of structures and functions of the attached proteins, thus changing the downstream biochemical processes throughout the cytoplasm and nucleus.[16]

The cytoskeleton is not the only example which shows the coupling of mechanics and biochemistry. Other examples include the folding of two or more globular clusters (domains) and the deformation or unfolding of the globular domains in the ECM protein fibronectin under stretching forces. When cells apply tensile or contractile forces to the ECM, fibronectins unfold and refold, respectively.[17] It has been proposed that the folding and unfolding states of fibronectins may have significant implications to cell signaling, since different fibronectin structures regulate the fibronectin–integrin binding or establish a mechanosensitive ligand recognition system.[18]

The elastic properties of DNA have also attracted attention due to DNA's importance in storing genetic information. The arrangement of the four DNA bases, i.e., adenosine, cytidine, guanosine and thymidine, provides the code to produce proteins. However, not all sequences encode genetic information. Some DNA sequences serve as recognition sites for DNA-binding proteins, like the TATA box,[19] which labels the starting position of transcription.[20] To understand why base sequences have specific affinities for certain proteins, the rigidity of DNA has

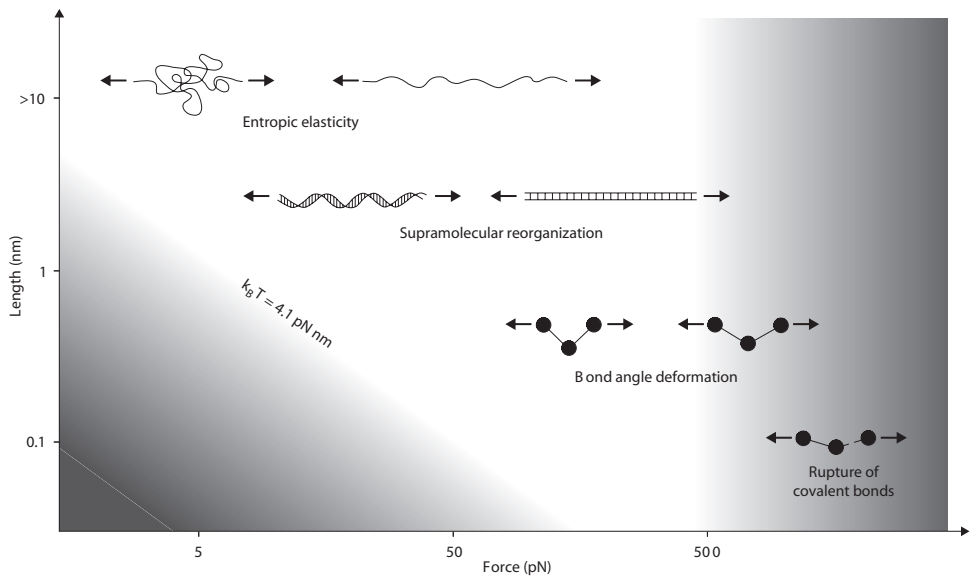

Fig. 2. Accessible force window of single-molecule manipulation.[34] The white area shows the experimental accessibility of mechanical information. From Ref. 34.

been studied extensively,[21–23] including the sequence dependence of the stiffness of DNA.[24–26]

1.2. *Single-molecule manipulation*

Since Feynman proposed the idea of the molecular machine in his famous speech *"There's Plenty of Room at the Bottom"* in 1959,[27] nanoscience and nanotechnology have advanced into technology-based research, opening the door for the precise manipulation of objects on the atomic scale. Recent developments in single-molecule manipulation have created new research in many fields such as physics, chemistry, materials science, biology, medicine and engineering. A number of techniques that can be applied to measure tiny forces are available: The most prominent of which are the AFM,[28,29] optical tweezers,[30] magnetic tweezers,[31] glass microneedles,[32] and the biomembrane force probe.[33] Within the accessible force window,[34] the range from measuring the entropic elastic force (several femtonewtons) to breaking covalent bonds (a few nanonewtons) can now be studied (Fig. 2).

1.2.1. *Atomic Force Microscopy (AFM)*

To improve the microscope resolution beyond the Abbé barrier of 200 nm using visible light, Binnig *et al.*, of IBM Zürich research laboratory, proposed a new scanning probe microscope in 1986, i.e. the AFM.[35] An AFM probe attached to an ultra-soft cantilever senses the force between atoms of the probe and the surface.

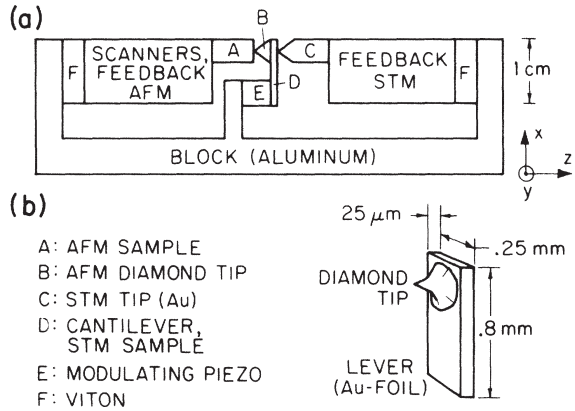

Fig. 3. Experimental set-up of the first generation AFM. From Ref. 35.

In the prototype AFM (Fig. 3), a scanning tunneling microscope (STM) probe monitored the bending of the cantilever, with a feedback control system which controlled the vertical movement of the scanner to keep the force on the AFM probe constant while it raster scanned over sample surfaces. The surface topography was then reconstructed from the vertical movement of the scanner. In 1987, a new method to measure the bending of the AFM cantilever based on the optical lever mechanism was proposed.[36] This optical system has now replaced STM probes as the most popular AFM probe displacement sensor.

When the operating force during AFM scanning is high, the interaction between the tip and the surface produces a deformation on soft film,[37] which inspired researchers to use AFM tips to manipulate microscopic objects. AFM tips were used to modify the surface[38,39] or to move nanomaterials to construct arbitrary nanoscale patterns.[40] This technique opened up new possibilities in manipulating materials for nanoscience and nanotechnology. Thus, the AFM is not only a detector, but also a nanostructure constructor and manipulator.

Taking advantage of the capability of AFM to measure the force applied onto the tip while manipulating the object, the first biological force measurement using AFM was demonstrated in 1994.[28] AFM tips were functionalized with avidin to measure the adhesive force of agarose beads modified with biotin to extract the avidin–biotin specific binding force. AFM was later used to investigate the mechanical and thermodynamic properties of biomolecules. For example, a giant sarcomere muscle protein was picked up by an AFM probe and stretched (Fig. 4). The force exerted on the molecule as a function of extension was recorded and the resulting sawtooth patterns were attributed to the unfolding of individual domains.[28]

Unlike optical tweezers, where the biomolecule was held between two beads *via* molecular handles, the AFM tip attaches to the biomolecule *via* nonspecific binding. This allows AFM to apply higher forces to the biomolecule than with optical tweezers. In addition, the force curve obtained using AFM does not include

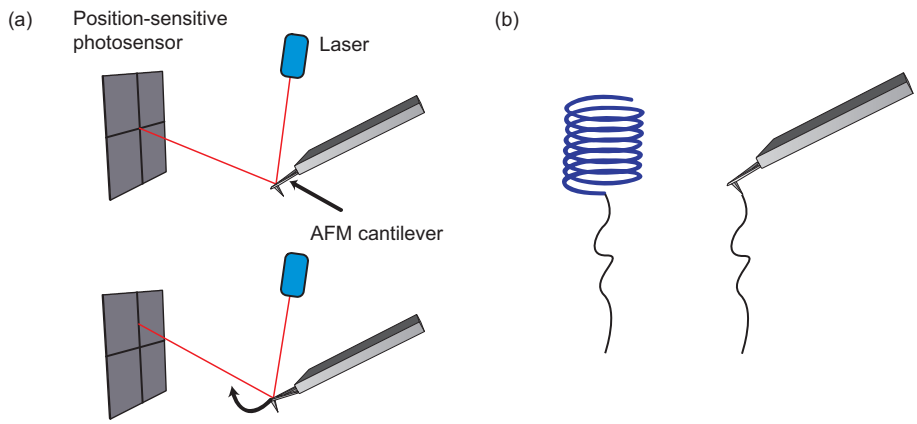

Fig. 4. Detection principles of AFM. (a) The bending of the AFM cantilever induced by the force applied to the tip is magnified and determined from the laser beam deflection on the position-sensitive photosensor. (b) The AFM cantilever is assumed to act as a harmonic potential that applies force onto a molecule. From measuring the vertical displacement of the cantilever and the spring constant, the force exerted on the molecule is calculated.

the contribution from the DNA handles, whereas in optical tweezers, the elastic properties of handle molecules must be decoupled from the force curves.

1.2.2. *Optical tweezers*

In 1987, Ashkin *et al.* first used optical tweezers to move cells under a damage-free condition.[41] Optical tweezers use the force generated by the radiation pressure of a focused laser light beam, with the gradient force keeping the micrometer size beads in the high intensity region of the light beam[42,43] (Fig. 5). This gradient force is effective in manipulating particles from the micrometer-scale particles down to individual atoms.[44,45] The first generation of the experimental set-up consisted of a 1.06 μm wavelength neodymium-doped yttrium aluminium garnet laser focused onto a viewing plane with a water-immersion objective lens to form a single-beam optical trap. After being trapped in the focal spot, the position of the biological cell can be controlled by moving the X,Y,Z microscope sample stage. Ashkin *et al.* also separated individual bacteria from one sample and introduced them into another, demonstrating the potential of performing cell surgery using this optical technique.[41]

Optical tweezers were used to measure the force-extension curves of individual double-stranded DNA (dsDNA) molecules in 1996.[30] Each end of the dsDNA molecule was coupled with a micrometer size latex bead, with one bead held by a glass micropipette and the other bead held in the optical trap. The dsDNA molecule was extended by moving the pipette away from the laser trap. The change in dsDNA length was monitored by recording the distance between two beads with a video camera. They adopted a new optical tweezer design where the force acting on

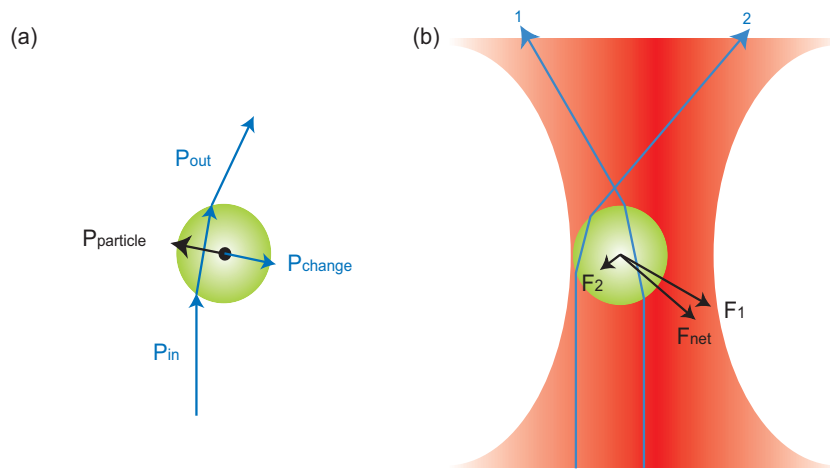

Fig. 5. The operating principles of optical tweezers.[41] (a) The change in scattering photon momentum ($P_{\text{change}} = P_{\text{out}} - P_{\text{in}}$) produces an opposite momentum change on the particle (P_{particle}) according to Newton's third law. (b) Different shades of red represent different intensities light. When the particle is displaced from the beam center, the net force of the radiation pressure exerted on the particle points toward the beam waist.

the dsDNA molecule corresponding to each extension could be directly determined from the angular intensity distribution of the laser beams on position-sensitive photodetectors.[46] Removing the need for complicated calibration,[47] this direct method to measure the force exerted by optical tweezers remains popular.

Recent developments have improved the stability and reduced the noise in optical tweezers.[48] Many hybrid systems have been proposed, significantly expanding the capabilities of traditional optical tweezers. These include multiple optical traps,[49] optical tweezers coupling with rotational control,[50] and fluorescence optical tweezers,[32] enabling the manipulation of more complex biological systems.

2. Methods

2.1. *AFM experiments*

2.1.1. *Sample preparation*

One way to obtain a clean gold substrate for an AFM substrate is to have an AFM specimen disc adhered to a commercial silicon wafer coated with a gold layer by epoxy glue, which is left to dry for one day (Fig. 6). The AFM specimen disc is then carefully peeled away from the silicon wafer prior to sample attachment.

To prepare the sample solution, the molecules are diluted with a buffer solution at 100 μg/ml concentration with 150 mM NaCl, similar to physiological conditions. For titin, the buffer is phosphate buffer saline (PBS) solution. For DNA, the buffer is tris-HCl buffer solution containing 1 mM EDTA. This concentrated sample is stored at -20°C. To use the sample for experiments, the frozen sample solution is

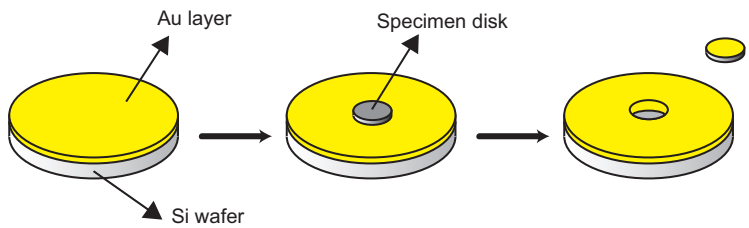

Fig. 6. Preparation of a clean gold substrate.

thawed and diluted to 10–50 μg/ml, in which 10 μl of the diluted solution is gently dropped onto a clean gold substrate. The sample is incubated for 15 minutes for titin and several hours or overnight for DNA. Finally, 1–2 ml buffer solution is used to rinse the substrate to remove unattached molecules. Additional buffer solution is added to the substrate to keep the sample in a fluid environment.

2.1.2. *Force measurement*

A clean AFM tip was used to pick up the individual molecule on the substrate by nonspecific adsorption, which has been shown to resist forces as large as 2 nN.[51] The molecule was attached between the tip and the substrate, and the extension of the tethered molecule was controlled by the vertical position of the substrate. For repeated pulling experiments, the substrate was first moved toward the tip until a repelling force between the tip and the substrate reached a preset value. Then the substrate was pulled away from the tip to a preset distance (Fig. 7(a)). For stretch-relaxation experiments, the tip is kept at least 100 nm above the substrate during each cycle to prevent the accidental attachment of another molecule to the tip. The force on the molecule was recorded as a function of time (Fig. 7(b)). For constant force experiments, the molecule was first stretched until the applied force reached a preset value and then the feedback-loop was turned on. The change in force triggered the stage movement to change the tip-substrate distance to keep the force constant (Fig. 7(c)).

2.1.3. *Calculation of extension*

The displacement of the piezo-stage, λ and the bending of AFM tip, were recorded as a function of time during experiments. The extension of the molecule, z, was obtained using,

$$z = \lambda - \Delta z\,, \tag{1}$$

where Δz is the AFM tip displacement from its equilibrium position. For both λ and Δz, positive values implied moving downward and negative values implied moving upward.

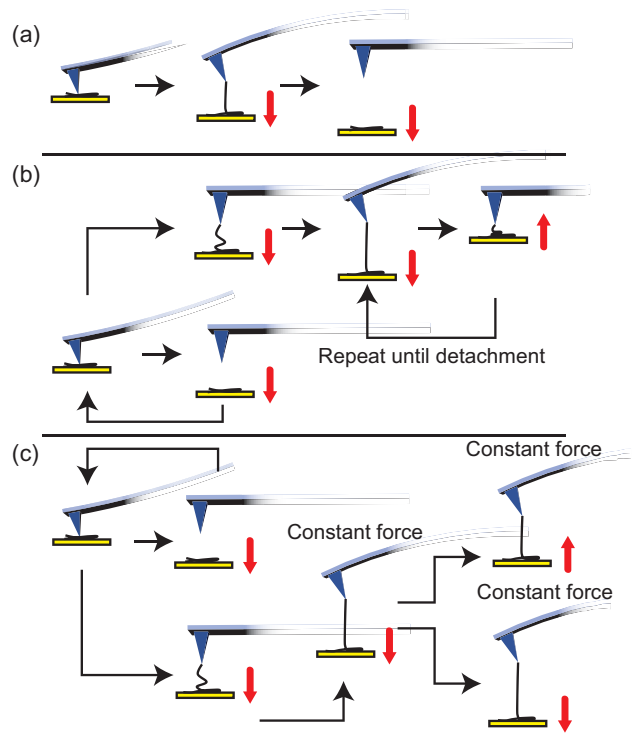

Fig. 7. (a) Typical pulling experiments where the movement of the substrate is controlled by the piezo-electric stage. (b) Stretch-relaxation experiments. After a molecule is picked up by the AFM tip, it is stretched and relaxed repeatedly. (c) Constant force experiments. A molecule is picked up and it is stretched until the force reaches a preset value and then the force is kept constant.

2.2. *Equilibrium free energy curve reconstruction*

2.2.1. *Jarzynski's equality*

Since stretching a molecule is not an equilibrium process, the free energy changes cannot be directly obtained by calculating the work applied to the molecule. However, in 1997, Jarzynski derived an equation which relates the work, W, to the free energy change, ΔG,[52]

$$\langle \exp(-\beta W) \rangle_{n\to\infty} = \exp(-\beta \Delta G)\,, \tag{2}$$

where $\beta \equiv 1/k_B T$, k_B is the Boltzmann constant, T is the temperature and $\langle \ldots \rangle_N$ is the average over N realizations. The equality is exact when $N \to \infty$, which indicates that the free energy change can be determined by the work done in single-molecule manipulation experiments.

2.2.2. *Velocity dependence*

Jarzynski's equality[52,53] shows great potential as a method for obtaining the free energy change from nonequilibrium single-molecule force-extension

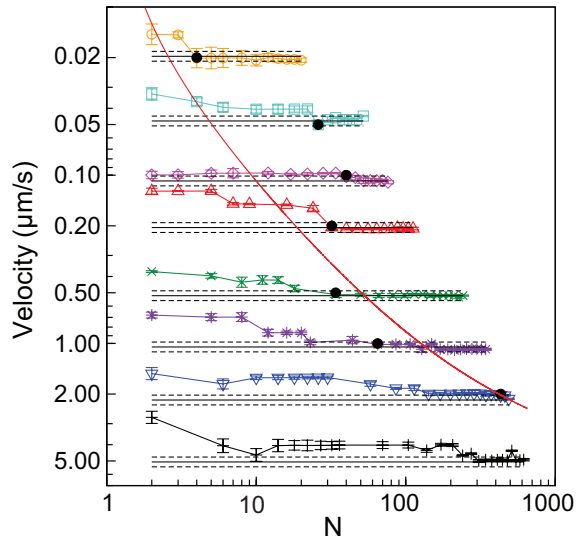

Fig. 8. Free energy convergence as a function of pulling velocity.[61] The number of realizations, N, required to converge to within 10% of the averaged free energy was found to depend exponentially on the pulling velocity. From Ref. 61.

measurements.[54−59] The equality promises to recover the free energy changes from single-molecule pulling experiments at any pulling velocity, given enough realizations.[60] However, the equality is strictly valid only in the limit of infinite realizations. Therefore, practical use of Jarzynski's equality requires that the number of realizations needed for an accurate approximation is reasonable for its practical application in experiments.

Figure 8 shows the number of realizations, N, necessary to calculate ΔG within 10% of the converged values as a function of pulling velocity.[61] N increases exponentially with velocity, so that excessively high pulling velocities call for impractical numbers of realizations.[60] High velocity results may also be affected by hydrodynamic drag.[62] On the other hand, pulling at very slow velocities introduces systematic error from instrument drift. Therefore, velocities between 0.2 μm/s and 1.0 μm/s appear to be optimal.[60]

2.2.3. *Is end-to-end distance a good reaction coordinate?*

While single-molecule manipulation has made much progress in recent years,[63,64] the important relationship between the thermal, mechanical and chemical process is still a subject of debate. The question is not whether the mechanical or chemical method more faithfully resembles the process *in vivo*, since both methods present results in the zero-perturbation limit, i.e. the zero force or zero chemical denaturant condition. The external perturbation changes the free energy landscapes, similarly for bulk chemical denaturants and single force measurements, implying that the

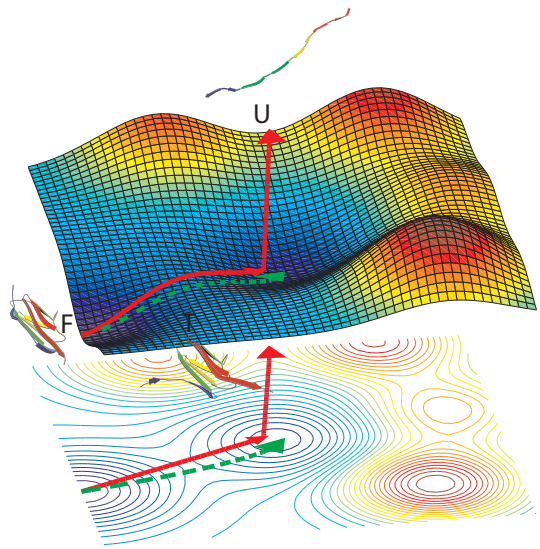

Fig. 9. The solid and dashed lines indicate the pathways of force and chemical induced unfolding, respectively.[60] Unlike chemical experiments, where the process is expressed in terms of the reaction coordinate, the force measurement has one additional constraint, i.e. the molecular end-to-end distance. From Ref. 60.

energy pathways of these two methods are close to each other (Fig. 9), thus supporting the notion that the end-to-end distance is a good reaction coordinate.

3. Application to Biomolecules

3.1. *Titin: Protein polymer physics and thermodynamics*

Titin is a giant protein responsible for generating passive retraction forces in muscle cells. This protein connects the M-line and Z-line of the sarcomere, stabilizing its structure and preventing it from being overstretched during muscle expansion. Titin consists of three spring elements: Ig (serially linked immunoglobulin-like domains), PEVK (rich in proline, glutamate, valine and lysine) and an N2B domain (only for cardiac muscles) (Fig. 10).[65,66] Several of the Ig domains, particularly, the I27 domains, have been studied extensively with the AFM [Fig. 11(a)] and optical tweezers.[67,68]

Figure 11(b) displays the force-extension curve of the titin $(I27)_8$ molecule. The first peak in the force curve can be attributed to the nonspecific binding force between the tip and the substrate. Upon stretching, the force increased with the movement of the substrate because of the entropy reduction resulting from the trend to align the molecule with the pulling direction. In the case of Fig. 11(b) where all eight domains were in the folded state before pulling, the globular domains were straightened without having initially unfolded.

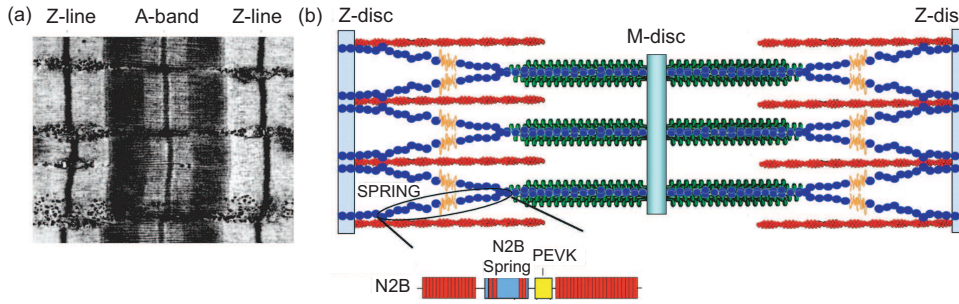

Fig. 10. (a) The electron micrograph of the sarcomere. Adapted from Ref. 65. (b) A schematic view of the sarcomere. Adapted from Ref. 66.

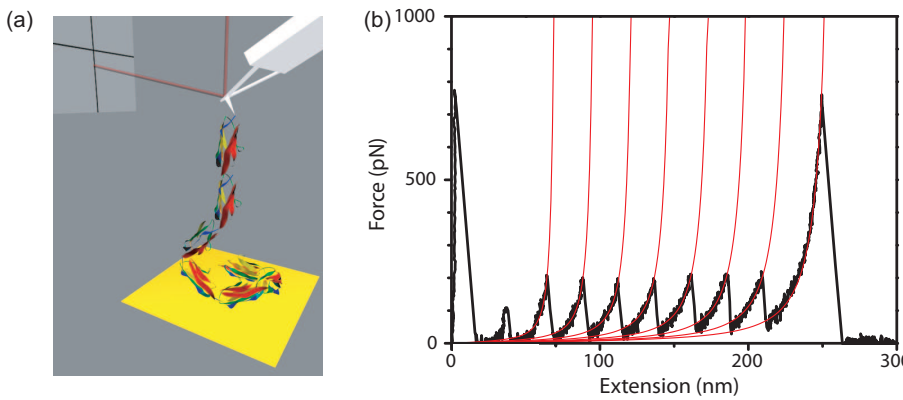

Fig. 11. (a) An illustration of titin $(I27)_8$ AFM force measurement.[60] The $(I27)_8$ protein is composed of eight titin immunoglobulin domains, I27. From Ref. 60. (b) The sawtooth pattern of an $(I27)_8$ protein force curve. Each peak represents the unfolding of one I27 domain. The ninth peak indicates the detachment of the titin protein from the tip or the substrate. Each unfolding peak is fitted to a WLC model curve.

The titin Ig-like I27 domains form a tertiary structure through intramolecular hydrogen bonds (Fig. 12). As the force applied to the molecule increased during the experiment, the bonds were distorted and the possibility of breaking the intramolecular interactions was increased. When one domain unfolded, the tension of the molecule suddenly dropped to show a down-stroke pattern on the force curve. Note that the force balance between the molecule and the tip does not hold in this region.

After the cantilever tip returned to the position where the force balance was established, the trace represents the straightening of the first unfolded domain. Without the enthalpic elasticity contribution of hydrogen bonds, the trace could be fitted with the standard wormlike chain (WLC) model, giving a good approximation

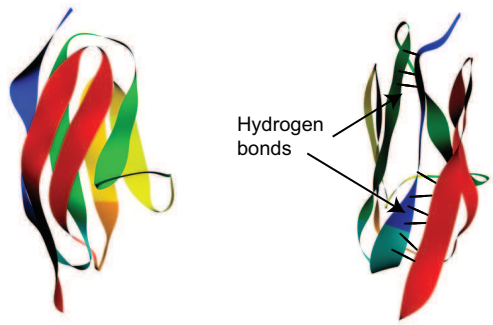

Fig. 12. Three-dimensional structure of the titin I27 protein.

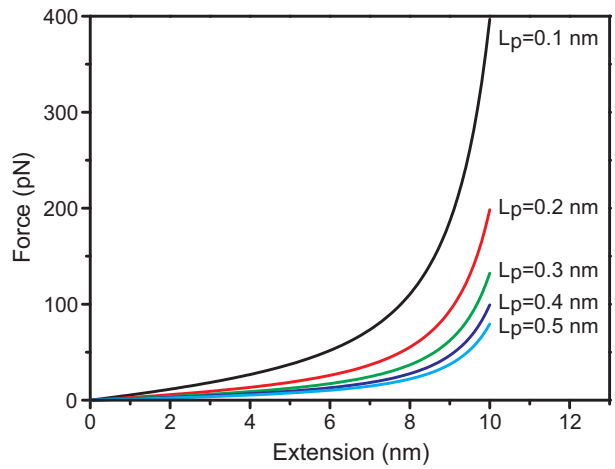

Fig. 13. Comparison of WLC model curves with respect to persistence length. The temperature is 300K and the contour length is 12 nm in the five WLC curves.

to describe the entropic elasticity of a polymer,[69]

$$\frac{FL_p}{k_BT} = \frac{z}{L_c} + \frac{1}{4(1-\frac{z}{L_c})^2} - \frac{1}{4}, \tag{3}$$

where F is the force, L_c is the contour length and L_p is the persistence length, a parameter describing the rigidity of a polymer (Fig. 13). In the case of titin, the persistence length is the size of one amino acid, 0.4 nm, and the contour length of each domain is 28 nm.[29,70]

As the molecule was extended, domains of a titin $(I27)_8$ molecule unfolded one by one, resulting in a sawtooth pattern. The last peak, [Fig. 11(b)], with a much higher force peak than the unfolding peaks, represents the detachment of the protein. Because the molecule is randomly picked up by the cantilever tip, not all the force-extension curves show the intact force curve like Figure 11(b). Figure 14 shows variations with fewer numbers of unfolding peaks and unfolding forces within

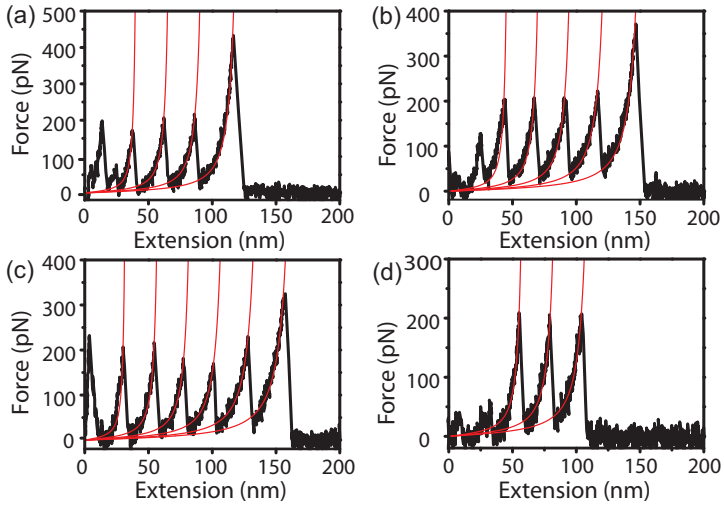

Fig. 14. Typical force-extension curves of a titin $(I27)_8$ molecule. The red lines are WLC model fits to the data.

the force curve. This indicates that the unfolding event is a stochastic process.[70] Considering the unfolding as a zero-order reaction, the lifetime of the distorted titin I27 domain,[71] τ, is,

$$\frac{1}{\tau} = k_u(F) \sim \exp \frac{-(\Delta G_u^{\ddagger} - F\Delta x^{\ddagger})}{k_B T}\,, \tag{4}$$

where $k_u(F)$ is the reaction rate constant, $\Delta G^{\ddagger}$ is the free energy barrier for unfolding and $\Delta x^{\ddagger}$ is the distance between the native and transition states. The probability of unfolding increases with increasing applied force.

The cross correlation function was used to align force-extension curves by shifting them along the extension-axis,

$$r = \frac{\sum_i [(x_f(i) - \langle x_f \rangle) \times (y_f(i-d) - \langle y_f \rangle)]}{\sqrt{\sum_i (x_f(i) - \langle x_f \rangle)^2} \sqrt{\sum_i (y_f(i-d) - \langle y_f \rangle)^2}}\,, \tag{5}$$

where x_f and y_f are two force curve fits to the WLC model. After the d for the maximum r was found, the force and extension data of y were shifted by d data points. This method has been used to align the force curve obtained from the same kind of molecule with different contour lengths.[54,57] The geometric error due to the deviation of the pulling direction from the vertical line normal to the substrate has proven to be less than 1%.[70] Therefore, the reproducibility of the titin force curve can be confirmed by the good overlap among the force-extension curves (Fig. 15).

Figure 16 depicts the statistics of the data. The average increase in contour length from the first to the second peak was 28 nm, which is close to the expected maximum length change of 29 nm from the unraveling of an I27 domain.[72,73] The analysis also shows that the domain length, defined as the peak-to-peak distance,

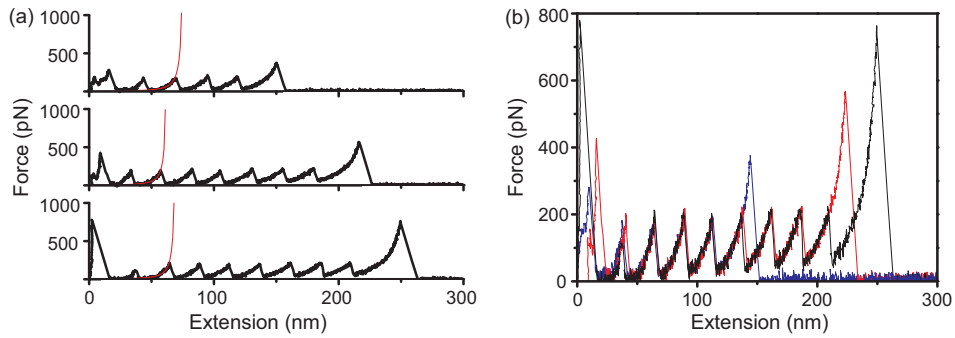

Fig. 15. Overlay of titin force-extension curves. The force-extension curve is shifted along the extension-axis according to cross correlation functions. The overlay shows that the second peaks of three selected force-extension curves are well overlapped.

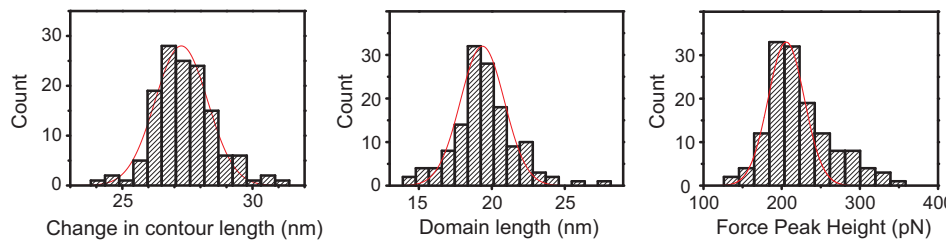

Fig. 16. Histograms of the contour length difference between the first and the second peak, length of the second domain, and the force of the second peak height. The contour length was obtained from WLC fitting curves. The pulling velocity is 1 μm/s.

20 nm, is shorter than the contour length. Thus, the unfolded chain could not fully extend before the next domain unfolded. At a pulling speed of 1 μm/s, the force peaks ranged from 120 to 350 pN, with an average force of 235 pN. The unfolding force depends on the mechanical stability of the folded molecule and pulling velocity.[54] Repeated pulling experiments show a distribution in force peaks. Stretch-relaxation of the same molecule eliminates the variety caused by the geometric error.[70] However, the molecule may fail to refold after several cycles, thereby increasing the difficulty in collecting a complete set of data.

Reconstruction of free energy surfaces was done using the method described in Ref. 54. In brief, the second peaks were extracted from a titin $(I27)_8$ force curve and aligned using cross correlation functions [see Eq. (6)]. Each of the N integration curves was split into S segments and the free energy difference between the starting point of the integration and the midpoint of the mth segment was calculated using,

$$\exp[-\beta\Delta G(z_m)] \approx \frac{1}{NS}\sum_{i=1}^{N}\sum_{j=1}^{S}\delta_\epsilon(z_m - z_{i,j}) \times \exp(-\beta W_{i,j})\,, \tag{6}$$

where $z_{i,j}$ is the extension of the molecule at the jth data point for the ith trajectory and $W_{i,j}$ is the work performed up to this data point. δ_ϵ is $1/\epsilon$ when $z_{i,j}$ falls inside

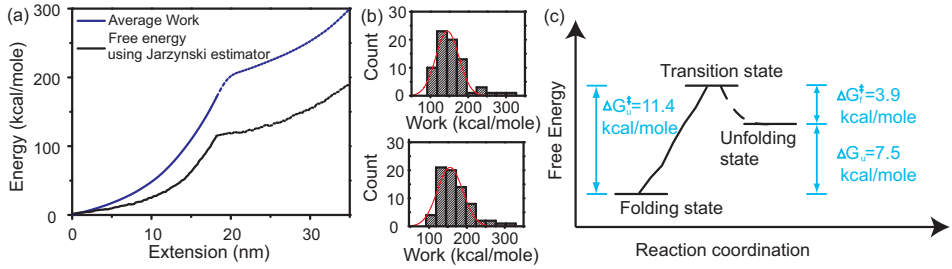

Fig. 17. Free energy curve of titin I27 proteins.[54] (a) The free energy curves were reconstructed using the Jarzynski's equality and arithmetic mean. (b) The distribution of the work done until 0.6 nm before the peak (upper) and at the peak (lower). (c) The free energy diagram of the titin unfolding/folding process. $\Delta G_u^{\ddagger}$ was obtained from the free energy surface reconstructed using Jarzynski's equality, assuming the distance between the folded and the transition states is 0.6 nm. Adapted from Ref. 54.

the mth segment and 0 otherwise. Figure 17 shows the reconstructed free energy curve along the end-to-end distance coordinate. The averaged work curve, $\langle W \rangle = \frac{1}{N}\Sigma_{i=1}^{N} W_i$ displayed in Fig. 17 for comparison, is about twice that of Jarzynski's averaged free energy curve.

Assuming the length difference between the native state and the transition state of I27 protein is 0.6 nm,[74] the energy barrier for unfolding, $\Delta G^{\ddagger}$, can be obtained from the free energy curve, 11.4 kcal/mole. In the downstoke region, the assumption that the force on the molecule equals the restoring force of the cantilever no longer holds. Therefore, the free energy curve is not accurate after the transition state. However, using the unfolding free energy change, $\Delta G_u = 7.5$ kcal/mol, determined by other equilibrium studies,[75] the energy barrier for folding, $\Delta G_f^{\ddagger}$, was determined to be 3.9 kcal/mole, which is in the expected range for I27, thus further validating this method.

3.2. *DNA mechanics and melting*

3.2.1. *Melting of double-stranded DNA*

AFM has also been used to study the mechanical melting of dsDNA, as shown in Fig. 18. λ-DNA is a dsDNA, having normal distributions of base sequences. Therefore, the segments randomly picked up by the AFM have no effect on the results. The force curves show two distinct features at 65 pN and near 150 pN, which are attributed to the B–S transition and dsDNA melting, respectively.[30,76–80]

The B–S transition is the transition from the B-form DNA to a metastable S-form. B-form DNA is the double helix structure formed by Watson–Crick base pairing. During pulling experiments, when the B-form λ-DNA is overstretched, the dsDNA no longer adopts the B-form structure and undergoes conformational changes including base unstacking and the unwinding of the helix structures.[30,78] The three conformations of λ-DNA during pulling, B-DNA, S-DNA

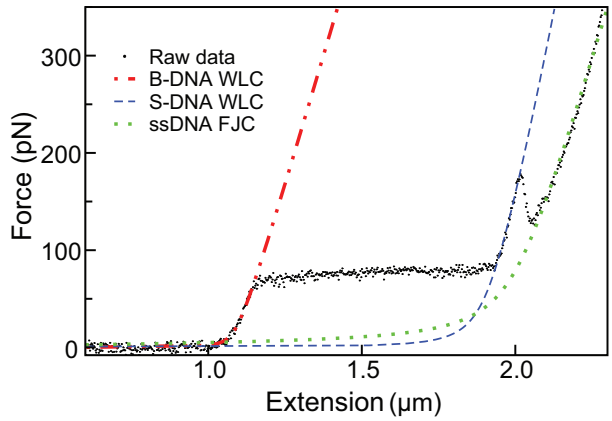

Fig. 18. Force-extension curve of dsDNA.[76] The dsDNA force curve is fitted to the extensible WLC and the extensible freely-jointed chain (FJC) models to describe three different conformations during stretching. *B*-DNA and *S*-DNA are fitted using the extensible WLC model with different parameters. Single-stranded DNA (ssDNA) is fitted using the extensible FJC model. From Ref. 76.

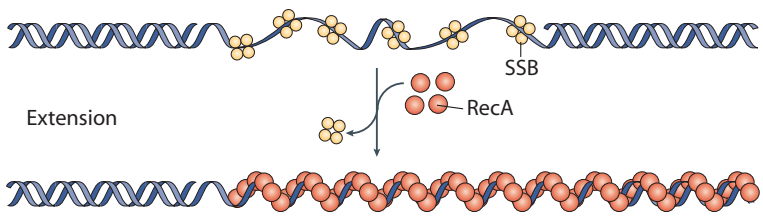

Fig. 19. During DNA recombination, dsDNA was coated by RecA proteins and was extended by 50% before the exchange of DNA strands and the homology search.[86] This process does not require ATP hydrolysis. Adapted from Ref. 86.

and ssDNA, can be described by the extensible WLC model and the extensible FJC model.

S-DNA may play an important role in DNA related reactions, such as those requiring lengthening by 50% of its contour length.[81,82] These conformational changes were achieved by coupling DNA with a variety of proteins. Considering the significant energy cost for stretching a WLC close to its contour length, how dsDNA is stretched beyond its contour length without adenosine triphosphate (ATP) hydrolysis (Fig. 19) presents a challenging problem. The force curve of dsDNA suggests that switching to an overstretched conformation might serve a much lower free energy pathway for lengthening.

3.2.2. *Stretching poly(dA)*

The unique conformational transition of poly(dA), an ssDNA, composed with only A bases, has also been revealed by AFM studies.[83,84] Unlike other ssDNA, such

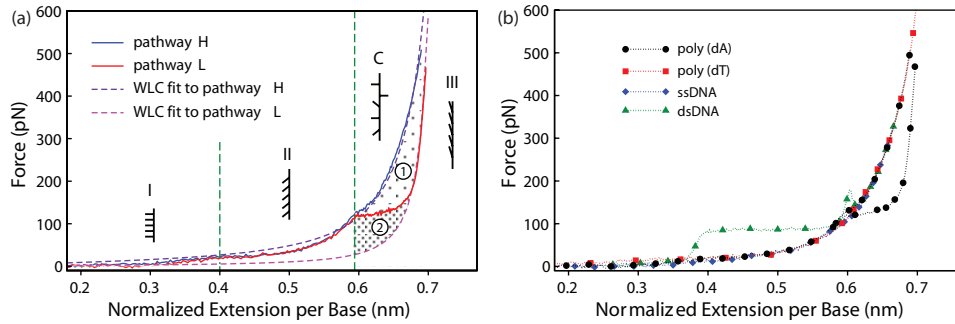

Fig. 20. Force-extension curves of poly(dA). (a) Force curve of poly(dA) separated into three sections. Areas 1 and 2 show the free energy difference. (b) Force curves of poly(dA), poly(dT) and λ-phage ssDNA and dsDNA. From Ref. 83.

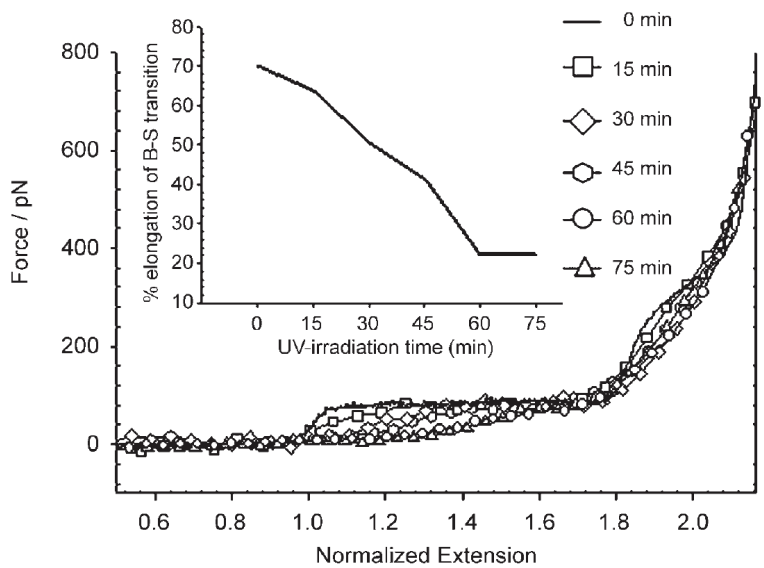

Fig. 21. Dose-dependent shortening of the *B–S* and second transitions of dsDNA. From Ref. 85.

as those composed of mixed bases and poly(dT), poly(dA) force-extension curves exhibit plateaus indicating unique phase transitions. The stretching and relaxing of poly(dA) exhibited two different stretching pathways at high forces:[83] A higher energy pathway, similar to ssDNA with a random base sequence, such as λ-DNA and poly(dT) [Fig. 20(b)] and a lower energy pathway showing an additional transition [Fig. 20(a)]. This indicates that the conformation of the higher energy pathway represents random coils and the energetically favored pathway represents a novel conformation of poly(dA), perhaps with unique stacking structures. The three different conformational regions of poly(dA) are illustrated in Fig. 20(a).

3.3. *Medical applications*

AFM has been used to quantify the effects of DNA damage, which has long been linked to the development of various cancers. For example, the effect of DNA damage by UV radiation on dsDNA's elastic properties has been investigated.[85] Results from force-extension curves of dsDNA irradiated with varying degrees suggest that increasing radiation damage resulted in the shortening of both the *B–S* and second transition of dsDNA (Fig. 21). The study shows that for the *B–S* transition, both the length of *B–S* transition shortened and the number of UV-induced cyclobutane pyrimidine dimer (CPD) lesions reached a maximum at a radiation dose of 40 kJ/m^2, suggesting that CPD lesions are responsible for the shortening of the *B–S* transition. These results demonstrate that CPD lesions may undermine the base interaction and even lead to DNA melting.

4. Conclusion

Single-molecule force measurements have become practical due to the recent advances in nanotechnology. The demonstrated applications indicate that single-molecule manipulation may be used to obtain information not accessible by traditional chemical methods and may serve as a useful tool for medical and biological research. Novel conformations and transient dynamics are now revealed by manipulating individual molecules. New developments in instrumentation, i.e. reduced noise and sophisticated pulling configurations such as dual AFM probes, new pulling schemes such as those triggering different biomolecule reactions, and advanced data analysis, e.g., using the nonequilibrium work theorem, will greatly extend the utility of the technique. Furthermore, rich information still lies under these dynamic measurements and a further understanding of the force data will provide us important knowledge of these systems.

Acknowledgments

We thank NSF DMR-0907676 and Welch Foundation C-1632, and NIH HL071895-06A1 for financial support.

References

1. N. Wang, J. P. Butler and D. E. Inger, *Science* **260**, 1124 (1993).
2. A. F. Oberhauser *et al.*, *Nature* **393**, 181 (1998).
3. D. A. Fletcher and R. D. Mullins, *Nature* **463**, 485 (2010).
4. G. Bao, *J. Mech. Phys. Solids* **50**, 2237 (2002).
5. C. Hahn and M. A. Schwartz, *Nat. Rev. Mol. Cell Biol.* **10**, 53 (2009).
6. J. H. Keyak *et al.*, *Bone* **44**, 449 (2009).
7. D. E. Jaalouk and J. Lammerding, *Nat. Rev. Mol. Cell Biol.* **10**, 63 (2009).
8. R. H. Christenson, *Clin. Biochem.* **30**, 573 (1997).
9. S. C. Manolagas and R. L. Jilka, *New Engl. J. Med.* **332**, 305 (1995).
10. J. S. Alwood *et al.*, *Bone* **47**, 248 (2010).

11. R. G. Bacabac *et al.*, *J. Biochem.* **41**, 1590 (2008).
12. J. L. Lucitti *et al.*, *Development* **134**, 3317 (2007).
13. E. D. Hay, *Cell Biology of Extracellular Matrix* (Plenum Press, New York, 1991).
14. M. E. Chicurel, C. S. Chen and D. E. Ingber, *Curr. Opin. Cell Biol.* **10**, 232 (1998).
15. J. S. Bennett *et al.*, *J. Biol. Chem.* **274**, 25301 (1999).
16. W. Guo and F. G. Giancotti, *Nat. Rev. Mol. Cell Biol.* **5**, 816 (2004).
17. T. Ohashi, D. P. Kiehart and H. P. Erickson, *Proc. Natl Acad. Sci. USA* **96**, 2153 (1999).
18. A. Krammer *et al.*, *Proc. Natl Acad. Sci. USA* **96**, 1351 (1999).
19. R. P. Lifton *et al.*, *Cold Spring Harb. Symp. Quant. Biol.* **42**, 1047 (1978).
20. S. T. Smale and J. T. Kadonaga, *Annu. Rev. Biochem.* **72**, 449 (2003).
21. P. J. Hagerman, *Annu. Rev. Biophys. Chem.* **17**, 265 (1988).
22. C. Bustamante, Z. Bryant and S. B. Smith, *Nature* **421**, 423 (2003).
23. A. A. Travers and J. M. T. Thompson, *Phil. Trans. R. Soc. A* **362**, 1265 (2004).
24. M. Hogan and R. H. Austin, *Nature* **329**, 263 (1987).
25. N. L. Goddard *et al.*, *Phys. Rev. Lett.* **85**, 2400 (2000).
26. M. M. Gromiha, *J. Biotech.* **117**, 137 (2005).
27. R. P. Feynman, *Engi. Sci.* **23**, 22 (1960).
28. E.-L. Florin, V. T. Moy and H. E. Gaub, *Science* **264**, 415 (1994).
29. M. Rief *et al.*, *Science* **276**, 1109 (1997).
30. S. B. Smith, Y. J. Cui and C. Bustamante, *Science* **271**, 795 (1996).
31. S. B. Smith, L. Finzi and C. Bustamante, *Science* **258**, 1122 (1992).
32. A. Ishijima *et al.*, *Cell* **92**, 161 (1998).
33. E. Evans, K. Ritchie and R. Merkel, *Biophys. J.* **68**, 2580 (1995).
34. H. Clausen-Schaumann *et al.*, *Curr. Opin. Chem. Biol.* **4**, 524 (2000).
35. G. Binnig, C. F. Quate and Ch. Gerber, *Phys. Rev. Lett.* **56**, 930 (1986).
36. Y. Martin, C. C. Williams and H. K. Wickramasinghe, *J. Appl. Phys.* **61**, 4723 (1987).
37. O. M. Leung and M. C. Goh, *Science* **255**, 64 (1992).
38. Y. Kim and C. M. Lieber, *Science* **257**, 375 (1992).
39. R. D. Piner *et al.*, *Science* **283**, 661 (1999).
40. T. Junno *et al.*, *Appl. Phys. Lett.* **66**, 3627 (1995).
41. A. Ashkin, J. M. Dziedzic and T. Yamane, *Nature* **330**, 769 (1987).
42. K. Svoboda and S. M. Block, *Annu. Rev. Biophys. Biomol. Struct.* **23**, 247 (1994).
43. A. Ashkin, *Phys. Rev. Lett.* **24**, 156 (1970).
44. A. Ashkin *et al.*, *Opt. Lett.* **11**, 288 (1986).
45. S. Chu *et al.*, *Phys. Rev. Lett.* **57**, 314 (1986).
46. S. B. Smith, Y. Cui and C. Bustamante, *Meth. Enzymol.* **361**, 134 (2003).
47. K. Visscher, S. P. Gross and S. M. Block, *IEEE J. Sel. Top. Quant. Elec.* **2**, 1066 (1996).
48. C. Bustamante, Y. R. Chemla and J. R. Moffitt, in *Single-Molecule Techniques: A Laboratory Manual* (Cold Spring Harbor Laboratory Press, New York, 2008).
49. R. T. Dame, M. C. Noom and G. J. L. Wuite, *Nature* **444**, 387 (2006).
50. Z. Bryant *et al.*, *Nature* **424**, 338 (2003).
51. H. Li *et al.*, *Adv. Mater.* **3**, 316 (1998).
52. C. Jarzynski, *Phys. Rev. Lett.* **78**, 2690 (1997).
53. G. Hummer and A. Szabo, *Proc. Natl Acad. Sci. USA* **984**, 3658 (2001).
54. N. C. Harris, Y. Song and C.-H. Kiang, *Phys. Rev. Lett.* **99**, 068101 (2007).
55. J. Liphardt *et al.*, *Science* **296**, 1832 (2002).
56. W. J. Greenleaf *et al.*, *Science* **319**, 630 (2008).
57. D. Collin *et al.*, *Nature* **437**, 231 (2005).

58. R. A. Nome *et al.*, *Proc. Natl Acad. Sci. USA* **104**, 20799 (2007).
59. F. Kienberger *et al.*, *Biomaterials* **28**, 2403 (2007).
60. E. Botello *et al.*, *J. Phys. Chem. B* **113**, 10845 (2009).
61. N. C. Harris and C.-H. Kiang, *Phys. Rev. E* **79**, 041912 (2009).
62. H. Janovjak, J. Struckmeier and D. J. Muller, *Eur. Biophys. J.* **34**, 91 (2005).
63. G. Lee *et al.*, *Nature* **440**, 246 (2006).
64. O. Braun, A. Hanke and U. Seifert, *Phys. Rev. Lett.* **93**, 158105 (2004).
65. L. Tskhovrebova and J. Trinick, *Nat. Rev. Mol. Cell Biol.* **4**, 679-689 (2003).
66. M. M. LeWinter and H. Granzier, *Circulation* **121**, 2137 (2010).
67. W. A. Linke *et al.*, *J. Mol. Biol.* **261**, 62 (1996).
68. M. S. Z. Kellermayer *et al.*, *Science* **276**, 1112 (1997).
69. P. C. Hiemenz and T. P. Lodge, *Polym. Chem.* (CRC Press, 2007).
70. M. Carrion-Vazquez *et al.*, jatProg. Biophys. Mol. Biol. **74**, 63 (2000).
71. C. Bustamante *et al.*, *Annu. Rev. Biochem.* **73**, 705 (2004).
72. H. P. Erickson, *Proc. Natl Acad. Sci. USA* **91**, 10114 (1994).
73. A. Soteriou *et al.*, *Proc. R. Soc. Lond. B* **254**, 83 (1993).
74. P. M. Williams *et al.*, *Nature* **422**, 446 (2003).
75. V. Grantcharova *et al.*, *Curr. Opin. Struct. Biol.* **11**, 70 (2001).
76. C. P. Calderon *et al.*, *J. Phys.: Condens. Matter* **21**, 034114 (2009).
77. M. Rief, H. Clausen-Schaumann and H. E. Gaub, *Nat. Struct. Biol.* **6**, 346 (1999).
78. C. P. Calderon *et al.*, *J. Mol. Recognit.* **22**, 356 (2009).
79. C. P. Calderon *et al.*, *J. Phys. Chem. B* **113**, 138 (2009).
80. H. Fu *et al.*, *Nucleic Acids Res.* **38**, 5594 (2010).
81. A. Stasiak, E. D. Capua and T. Koller, *J. Mol. Biol.* **151**, 557 (1981).
82. K. Dunn, S. Chrysogelos and J. Griffith, *Cell* **28**, 757 (1982).
83. W.-S. Chen *et al.*, *Phys. Rev. Lett.* **105**, 218104 (2010).
84. C. Ke *et al.*, *Phys. Rev. Lett.* **99**, 018302 (2007).
85. G. Lee *et al.*, *Small* **3**, 809 (2007).
86. M. M. Cox, *Nat. Rev. Mol. Cell Biol.* **8**, 127 (2007).